Biomaterials Science

PAPER

View Article Online
View Journal | View Issue

Cite this: *Biomater. Sci.*, 2020, **8**, 266

Clickable, acid labile immunosuppressive prodrugs for *in vivo* targeting†

Hua Wang,[a,b] Miguel C. Sobral,[a,b] Tracy Snyder,[b] Yevgeny Brudno,[a,b] Vijay S. Gorantla*[c] and David J. Mooney*[a,b]

Received 15th September 2019,
Accepted 30th October 2019

DOI: 10.1039/c9bm01487j

rsc.li/biomaterials-science

Allotransplantation offers the potential to restore the anatomy and function of injured tissues and organs, but typically requires life-long, systemic administration of immunosuppressive drugs to prevent rejection, which can result in serious complications. Targeting the immunosuppressive drug to the graft favors local tissue concentration *versus* systemic drug exposure and end-organ toxicity. This could reduce the overall dose and dosing frequency of immunosuppressive drugs, and improve the safety and efficacy of treatment. Here, we developed dibenzocyclooctyne (DBCO)-modified prodrugs of the immunosuppressive drugs tacrolimus, rapamycin and mycophenolic acid, and demonstrated their targeted conjugation both *in vitro* and *in vivo* to azido-modified hydrogels *via* Click chemistry. Such azido-modified hydrogels placed in transplanted tissues enable sustained local release of drugs, and could be repeatedly refilled with systemically administered acid-labile prodrugs after drug exhaustion. Thus, clickable prodrugs with degradable linkers provide new possibilities for graft targeted immunosuppression in the context of allotransplantation.

Introduction

The technical, immunologic and functional feasibility of reconstructive transplantation as a promising treatment option for injured tissues has been established in over 200 procedures performed worldwide, including 145 upper extremity (hand), 42 face, and 26 uterus transplants (with over 10 live births).[1] Yet, the long-term risks of high-dose or multi-drug systemic immunosuppression remain the key obstacle to life-saving and life-enhancing benefits of such procedures.[2,3] Although it has been 65 years since the first kidney transplant was performed by a plastic surgeon, systemic, orally delivered immunosuppression with one or more drugs, remains the standard of care requirement to prevent rejection after transplantation.[4,5] The mainstay drug, tacrolimus (FK506, Prograf®), binds to intracellular FKBP-12 receptors and inhibits calcineurin, thus inhibiting interleukin-2 (IL-2) signaling and T cell activation.[6] Rapamycin (sirolimus, Rapamune®) suppresses the activation of T and B cells and vascular smooth muscle cell proliferation by inhibiting the mammalian target of rapamycin (mTOR).[7–10] Mycophenolate mofetil (MMF, Cellcept®) and its active prodrug mycophenolic acid (MPA), selectively block T-cell proliferation and suppress B-cell antibody production by suppressing guanosine-5′-monophosphate.[11–14] Unlike tacrolimus, which is mostly effective in acute rejection, rapamycin and MPA have superior efficacy in chronic rejection.[11–13,15–18]

Orally administered immunosuppressive drugs undergo extensive metabolism in the gastrointestinal tract and liver, greatly reducing their bioavailability. For example, bioavailability of oral tacrolimus is only between 7.3% to 19.7%.[19] Taking possible renal clearance into consideration, only a small percentage of drug typically reaches target graft tissues. Thus, drug levels in the bloodstream do not reliably or proportionally correlate with drug concentrations in graft tissues, and acute rejection can occur even when drug levels in the bloodstream are within the "target range".[19–23] For anti-rejection efficacy, large and repeated dosing of immunosuppressive drugs is often necessary, leading to high systemic drug exposure and increased risks of metabolic derangement, infections or malignancy.[24–26] Studies have shown that drug levels in the graft tissues are better correlates and monitors of dosing, exposure and efficacy.[19,27] Since the graft is the site of the initiation and perpetuation of the innate and adaptive immune response, it may be logical to direct and concentrate the immunosuppressive agents to the graft tissues.

[a]*Harvard John A. Paulson School of Engineering and Applied Sciences, Harvard University, Cambridge, Massachusetts 02138, USA. E-mail: mooneyd@seas.harvard.edu*
[b]*Wyss Institute for Biologically Inspired Engineering, Cambridge, Massachusetts 02138, USA*
[c]*Surgery, Ophthalmology and Bioengineering, Wake Forest School of Medicine, Winston-Salem, NC 27101, USA. E-mail: vgorantl@wakehealth.edu*

† Electronic supplementary information (ESI) available: ESI Fig. S1–S13. See DOI: 10.1039/c9bm01487j

Different from solid organ transplants that are internal, hand or face transplants are externally visible and accessible for diagnostic and treatment interventions, like topical immunosuppression or graft implanted drug delivery systems.[28] Graft implanted drug depots could bypass the intestinal/liver metabolism, and enable tunable release of single or multiple drugs over days to weeks. This spatiotemporal control over drug availability could reduce or eliminate risks of systemic drug exposure, drug–drug interactions and toxicity.[29–31] However, current implantable drug-eluting systems have a finite drug payload, inevitably requiring repeated administration of drugs or drug depots over time. For example, a single dose, tacrolimus-loaded gel injected into the limb transplants could prolong transplant survival for >100 days in rodent and porcine models, but eventually was depleted of drugs which led to graft rejection.[32,33] Albeit the great promise and clinical translatable potential of local drug depots, there is currently no noninvasive technique to refill these depots once their payload is depleted. Surgical or invasive replacement or repeated administration is typically needed, but could cause graft inflammation and rejection. To address limitations of current approaches, we developed, for the first time, clickable and degradable immunosuppressive prodrugs that enable timely and repeated conjugation to biomaterials or implants *via* efficient Click chemistry, and allow for minimally invasive loading of depots previously placed in a tissue. We have previously demonstrated the feasibility of targeting and conjugating chemotherapeutic prodrugs to a hydrogel depot, in the context of cancer treatment.[34,35]

In the current study, prodrugs were designed to contain a clickable head, a water-soluble segment, and a degradable linker responsive to either pH, redox, enzymes or other triggers indicative of tissue rejection. The release of the water-soluble prodrug could then be autonomously increased from a baseline level if tissue rejection, as indicated by the level of the trigger agent (*e.g.*, lower pH at the site of inflammation), is initiated. Both tacrolimus and rapamycin contain ketone groups for coupling of hydrazides and hydroxyl groups for esterification. Considering the much milder reaction conditions and the resulting acid-labile hydrazone bonds,[36,37] hydrazide-ketone chemistry was utilized for synthesizing prodrugs of tacrolimus and rapamycin. On the other hand, MPA contains a hydroxyl group that can be converted to carbonates for the development of acid-labile prodrugs. For the clickable head, dibenzocyclooctyne (DBCO) was introduced to all drugs as it can react with azido groups *via* efficient Click chemistry. The copper-free Click chemistry between azide and DBCO has been widely used for *in vivo* applications, due to the high reaction efficiency and bioorthogonality under physiological conditions, small size of azides, and high stability of both azides and DBCO.[38,39] Polyethylene glycol (PEG) was used as the water-solubilizing segment to enable pro-drugs to circulate in the body, diffuse into tissues, and bind to the hydrogel depot. To our knowledge, this is the first report of synthesis and characterization of DBCO-bearing prodrugs of tacrolimus, rapamycin and MPA, and their pH-dependent release profiles, pharmacokinetics, and Click chemistry-mediated targeting to azido-modified alginate hydrogels *in vitro* and after *in vivo* tissue implantation.

Results and discussion

We first modified rapamycin with clickable DBCO *via* a cleavable linker, while improving the drug water solubility. Rapamycin contains three hydroxyl groups that allow for esterification and two ketone groups that enable conjugation of hydrazides (Fig. 1a). Esterification requires a potent nucleophilic catalyst or high temperature, making site-specific modification of hydroxyl groups difficult. In contrast, the coupling reaction between ketones and hydrazides with weak acids as the catalyst can be efficient under much milder conditions. Rapamycin was first conjugated with *N*-β-maleimidopropionic acid hydrazide (BMPH) to yield rapamycin-mal with a maleimide ending group (Fig. 1a), which was confirmed by high performance liquid chromatography (HPLC) and mass spectrometry (MS) (Fig. S1†). DBCO-PEG_{1k}-SH was obtained *via* the amine-carboxyl coupling reaction between DBCO-NHS and NH_2-PEG_{1k}-SH (Fig. 1a and S2†), which further reacted with rapamycin-mal to obtain DBCO-PEG_{1k}-hydrazone-rapamycin (DBCO-hz-rapa, Fig. 1a). This reaction was validated *via* HPLC (Fig. 1b), and the structure of DBCO-hz-rapa was characterized by mass spectrum (Fig. 1c) and ^{1}H NMR spectrum (Fig. 1d). DBCO-hz-rapa showed excellent water-solubility (>100 mg mL^{-1}), and can be hydrolyzed into rapamycin in a pH-dependent manner, with faster reaction kinetics under pH 5.5 in comparison to pH 7.4 (Fig. 1e). To confirm its clickable property, DBCO-hz-rapa was incubated with azido-functionalized alginate (alginate-N_3, Fig. S3†). HPLC confirmed the complete consumption of DBCO-hz-rapa within 10 min (Fig. 1f), substantiating efficient Click chemistry-mediated conjugation. It is noteworthy that roughly 100 azido groups were conjugated to each alginate strand for the alginate-N_3 used in this study.[40]

Similarly, tacrolimus bearing a ketone group was first conjugated with BMPH to yield tacrolimus-mal (Fig. 2a and S4†), which further coupled with DBCO-PEG_{1k}-SH to yield DBCO-PEG_{1k}-hydrazone-tacrolimus (DBCO-hz-tacro) (Fig. 2a). The reaction was confirmed *via* HPLC (Fig. 2b), and the chemical structure of DBCO-hz-tacro was well characterized by mass spectrum (Fig. 2c) and ^{1}H NMR spectrum (Fig. 2d). DBCO-hz-tacro also showed excellent water solubility (>100 mg mL^{-1}), and can be degraded into tacrolimus in a pH-dependent manner, with a faster release of tacrolimus under pH 5.5 in comparison to pH 7.4 (Fig. 2e). The ability of DBCO-hz-tacro to covalently conjugate to alginate-N_3 *via* efficient Click chemistry was also validated by HPLC (Fig. 2f).

In contrast to rapamycin and tacrolimus, MPA only contains a hydroxyl group and a carboxyl group for functionalization (Fig. 3a). To avoid self-crosslinking, we converted the hydroxyl group into a carbonate by reacting with 4-nitrophenyl chloroformate, as confirmed by HPLC and mass spectrum (Fig. S5†). In parallel, DBCO-PEG_{1k}-OH was synthesized *via*

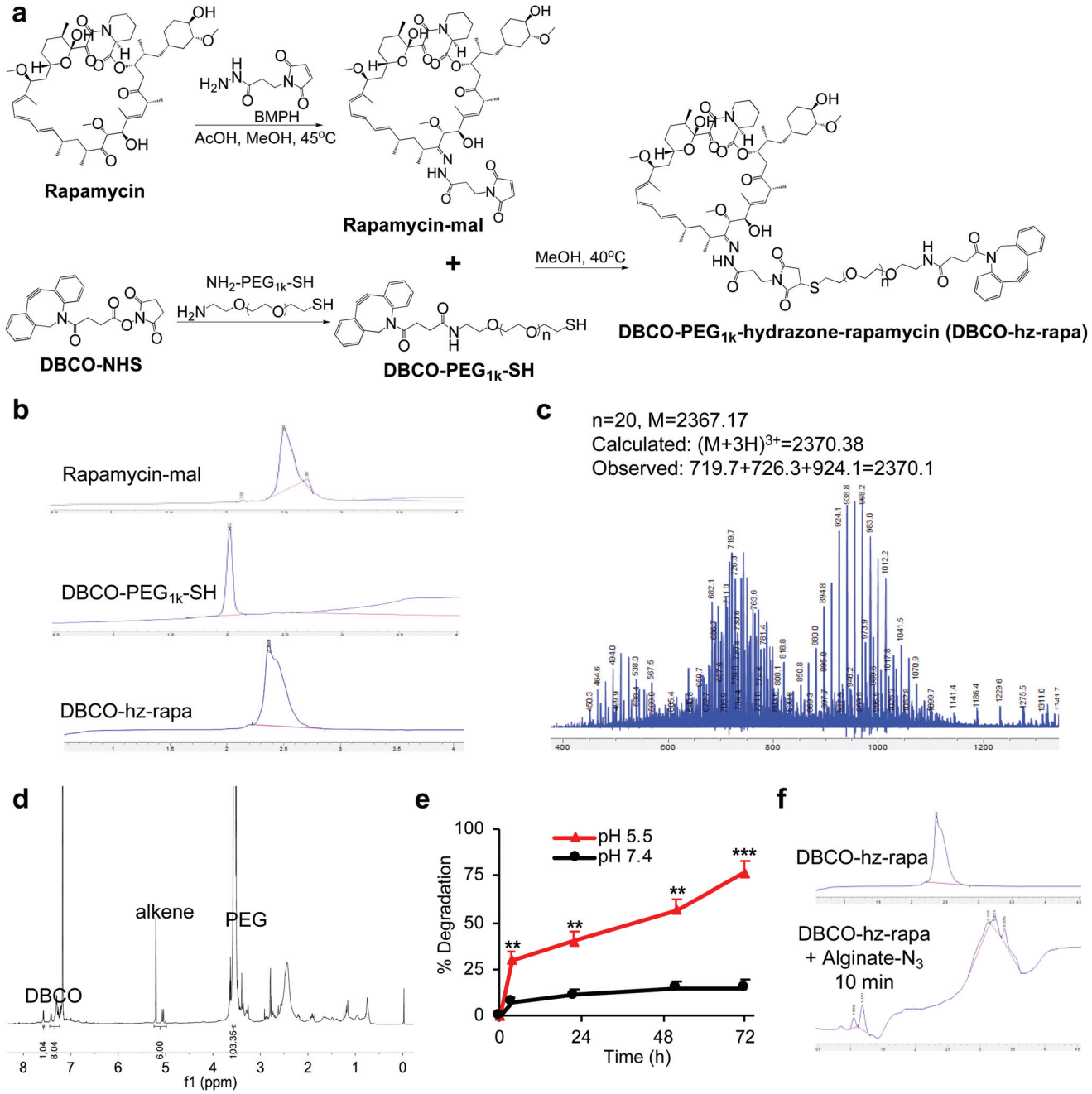

Fig. 1 Synthesis and characterizations of Clickable, acid labile DBCO-hz-rapa. (a) Synthetic route of DBCO-hz-rapa. (b) HPLC profiles of rapamycin-mal, DBCO-PEG_{1k}-SH, and DBCO-hz-rapa, respectively. (c) Mass spectrum of DBCO-hz-rapa. The interval of 14.7 (*m*/*z*) indicates the existence of $[M + 3H]^{3+}$. (d) ^1H NMR spectrum of DBCO-hz-rapa. (e) pH-Dependent degradation profiles of DBCO-hz-rapa to rapamycin under pH 7.4 and 5.5, respectively. Data were presented as mean ± SD (n = 4), and analyzed by two-tailed t-test ($0.01 < {*}P \leq 0.05$; ${**}P \leq 0.01$; ${***}P \leq 0.001$). (f) HPLC traces of the mixture of DBCO-hz-rapa and alginate-N_3, which showed rapid conjugation *via* Click chemistry.

coupling of NH_2-PEG_{1k}-OH and DBCO-NHS (Fig. 3a and b). The nucleophilic attack of MPA-4-nitrophyenyl carbonate by DBCO-PEG_{1k}-OH successfully yields DBCO-PEG_{1k}-carbonate-MPA (DBCO-MPA) (Fig. 3b), as confirmed by mass spectra (Fig. 3c). DBCO-MPA with a high water-solubility (>250 mg mL^{-1}) could be hydrolyzed to MPA in a pH-dependent manner (Fig. 3d). Similar to DBCO-hz-rapa and DBCO-hz-tacro, DBCO-MPA covalently conjugated to alginate-N_3 *via* Click chemistry (Fig. 3e).

After developing Clickable, acid-labile DBCO-hz-rapa, DBCO-hz-tacro, and DBCO-MPA, and demonstrated their capability to covalently conjugate to alginate-N_3 polymer, we next studied whether alginate-N_3 gels, formed by crosslinking of alginate-N_3 polymer chains *via* calcium ions, can first capture

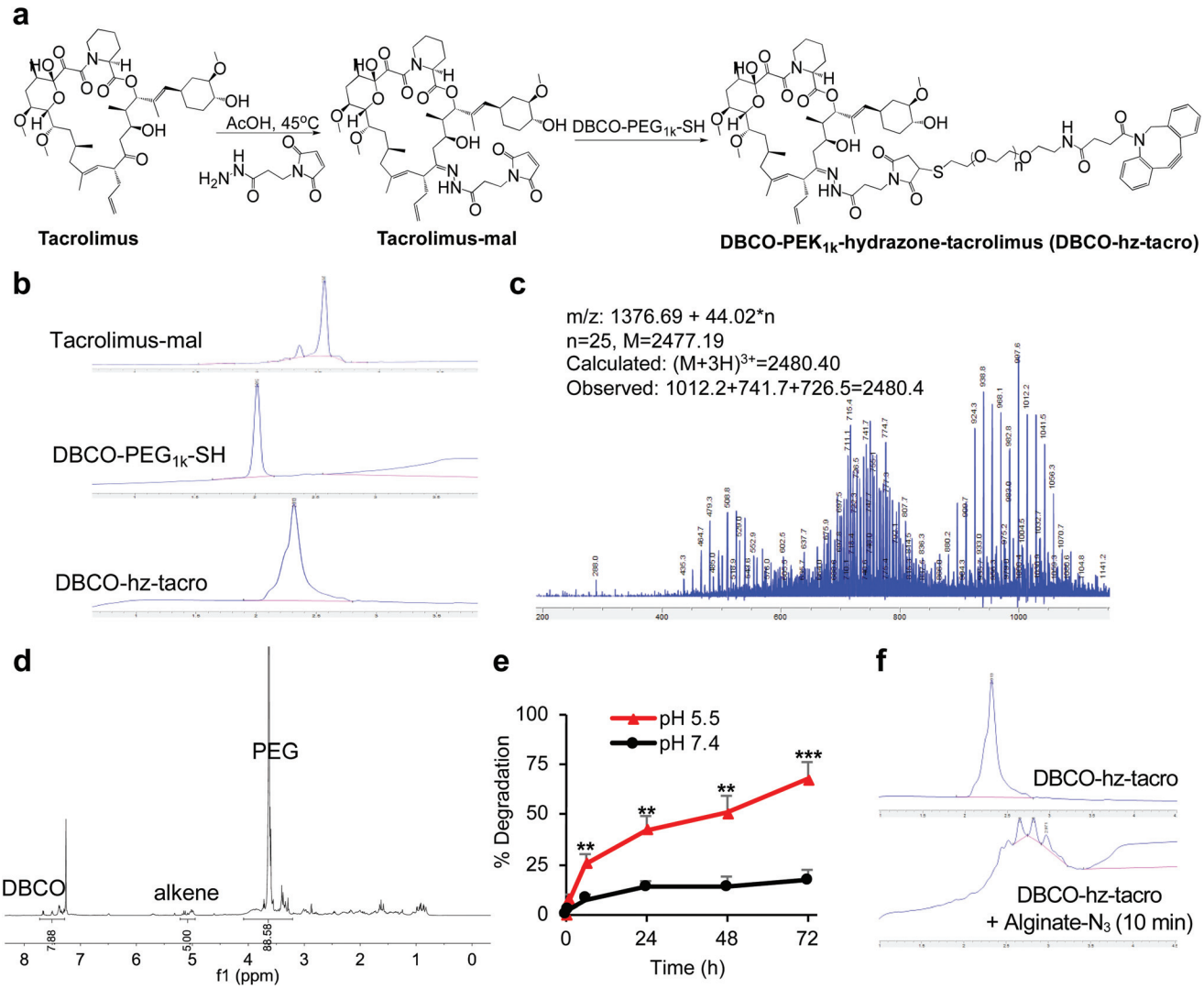

Fig. 2 Synthesis and characterizations of clickable, acid labile DBCO-hz-tacro. (a) Synthetic route of DBCO-hz-tacro. (b) HPLC profiles of tacrolimus-mal, DBCO-PEG_{1k}-SH, and DBCO-hz-tacro, respectively. (c) Mass spectrum of DBCO-hz-tacro. The interval of 14.7 (*m*/*z*) indicates the existence of $[M + 3H]^{3+}$. (d) ^{1}H NMR spectrum of DBCO-hz-tacro. (e) pH-Dependent degradation profiles of DBCO-hz-tacro to tacrolimus under pH 7.4 and 5.5, respectively. Data were presented as mean ± SD (n = 4), and analyzed by two-tailed t-test ($0.01 < {}^{*}P \leq 0.05$; $^{**}P \leq 0.01$; $^{***}P \leq 0.001$). (f) HPLC traces of the mixture of DBCO-hz-tacro and alginate-N_3, which showed rapid conjugation *via* Click chemistry.

these prodrugs and subsequently release the immunosuppressive drugs in a controlled manner (Fig. 4a). Alginate-N_3 gels were prepared by mixing a 2% (w/v) alginate-N_3 solution and a slurry of calcium sulfate for 45 min, and casting into cylindrical discs. Unmodified alginate gels were used as controls. After incubating gels with an aqueous solution of DBCO-hz-rapa, residual DBCO-hz-rapa in the solution was quantified *via* LC-MS. Alginate-N_3 gels captured 26% of the DBCO-hz-rapa in solution within 5 minutes, which compared to less than 2% captured by control gels (Fig. 4b). At 30 min, 35% and 2% of solution DBCO-hz-rapa was captured by alginate-N_3 and control alginate gels, respectively (Fig. 4b). The loading of DBCO-hz-rapa approached saturation after 3 h in both alginate-N_3 and control alginate gels, and alginate-N_3 gels exhibited ~2-fold greater loading than control gels (Fig. S6†). The loading of control gels with DBCO-hz-rapa is expected to result from simple diffusion of the molecule into the hydrogel from the surrounding solution, which increased over time as expected. In comparison, water-insoluble rapamycin showed minimal diffusion into alginate-N_3 gels (Fig. S7†). Following the loading study, the release kinetics of rapamycin from DBCO-hz-rapa conjugated alginate-N_3 gels was characterized under different pH conditions. Alginate-N_3 gels slowly released rapamycin over a course of >40 days, with faster release kinetics under pH 5.5, in comparison to pH 7.4 (Fig. 4c), presumably because of pH-dependent cleavage of the hydrazone linker of DBCO-hz-rapa. In contrast, control alginate gels exhibited fast release of the diffusively loaded DBCO-hz-rapa under neutral conditions, with over 70% being released within 72 h (Fig. S8†), demonstrating the importance of covalent con-

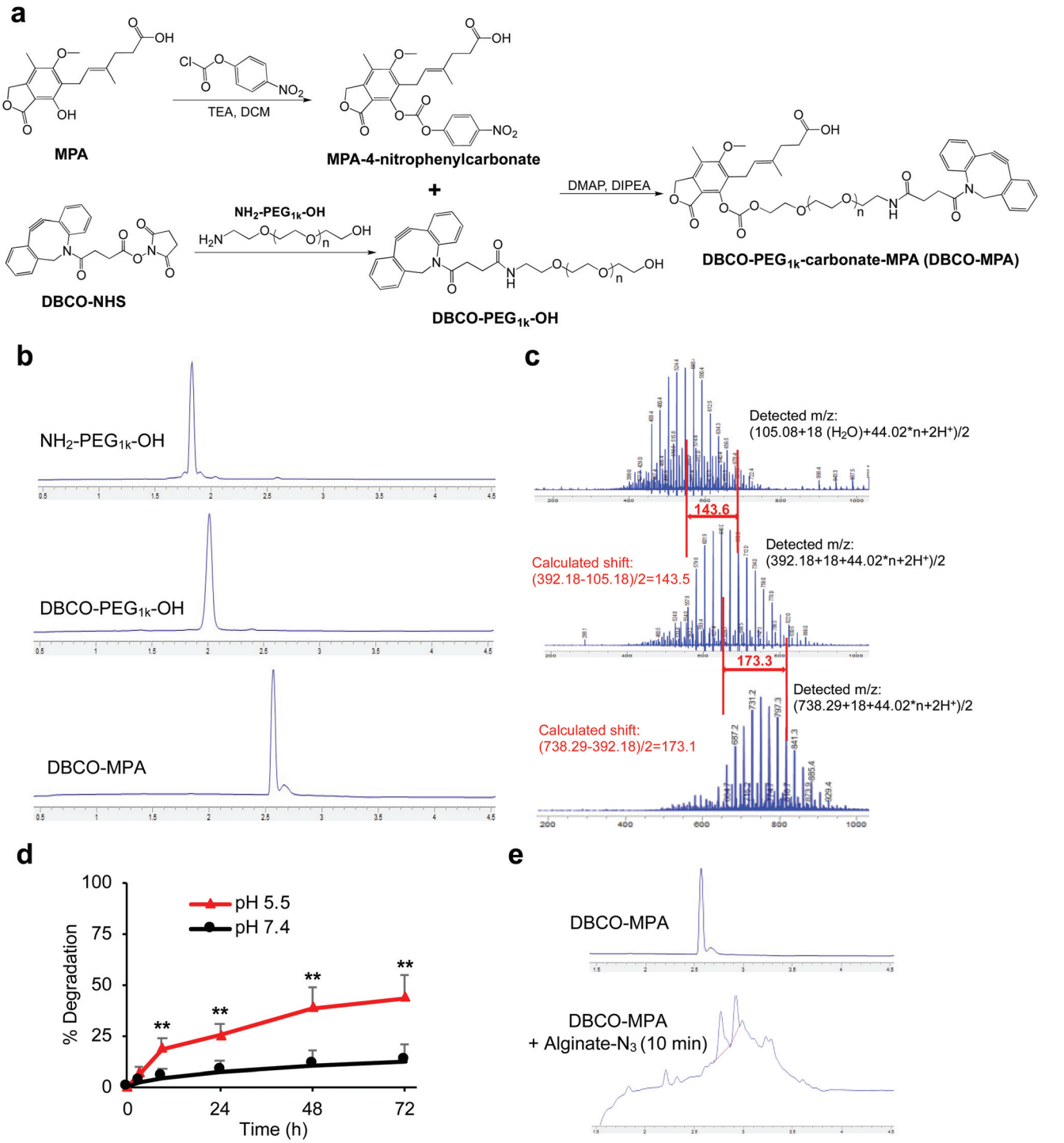

Fig. 3 Synthesis and characterizations of clickable, acid labile DBCO-MPA. (a) Synthetic route of DBCO-MPA. (b) HPLC profiles of NH_2-PEG_{1k}-OH, DBCO-PEG_{1k}-OH, and DBCO-MPA, respectively. (c) Mass spectra of NH_2-PEG_{1k}-OH, DBCO-PEG_{1k}-OH, and DBCO-MPA, respectively. The interval of 22 (*m*/*z*) indicates the existence of $[M + 2H]^{2+}$. (d) pH-Dependent degradation profiles of DBCO-MPA to MPA under pH 7.4 and 5.5, respectively. Data were presented as mean ± SD (n = 4), and analyzed by two-tailed *t*-test ($0.01 < {*}P \leq 0.05$; $**P \leq 0.01$; $***P \leq 0.001$). (e) HPLC traces of the mixture of DBCO-MPA and alginate-N_3, which showed rapid conjugation *via* Click chemistry.

jugation to achieve sustained release of these free drugs over a long period.

Similar to DBCO-hz-rapa, DBCO-hz-tacro was also rapidly captured by alginate-N_3 gels *via* efficient Click chemistry, with 5.7-fold and 2.9-fold increases in loading compared to control alginate gels after 1 h and 2 h, respectively (Fig. 4d). The alginate-N_3 gels captured 160% more DBCO-hz-tacro than control gels after 24 h (Fig. S9†). DBCO-hz-tacro conjugated alginate-

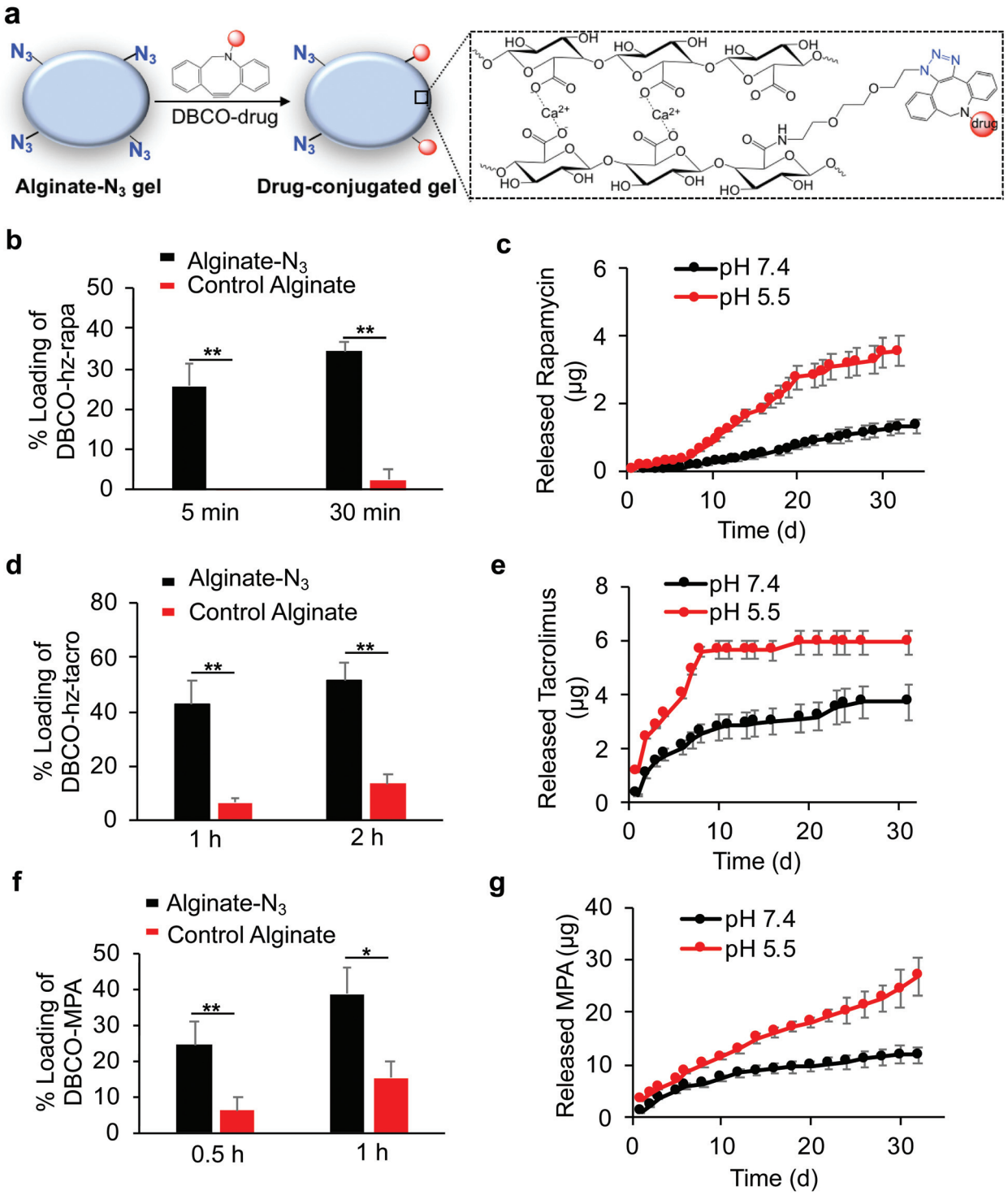

Fig. 4 Targeted loading of DBCO-hz-rapa, DBCO-hz-tacro, and DBCO-MPA to alginate-N_3 gels *via* Click chemistry and subsequent drug release kinetics. (a) Schematic illustration of coupling of DBCO-drugs with alginate-N_3 gels. Gels (2 mm height, 4 mm diameter) in 24-well plates were incubated with prodrugs in DMEM at 37 °C. At different time points, 10 μL of medium was taken out to quantify unconjugated DBCO-drugs. After 24 h, gels were placed in fresh medium to monitor the release of active drugs. (b) Loading of DBCO-hz-rapa into alginate-N_3 and unmodified alginate gels, respectively after 5 min or 30 min incubation (n = 4). (c) Release kinetics of rapamycin from alginate-N_3 gels at pH 5.5 and pH 7.4, respectively (n = 4). (d) Loading of DBCO-hz-tacro into alginate-N_3 and unmodified alginate gels, respectively after 1 h or 2 h incubation (n = 4). (e) Release kinetics of tacrolimus from alginate-N_3 gels at pH 5.5 and pH 7.4, respectively (n = 4). (f) Loading of DBCO-MPA into alginate-N_3 and unmodified alginate gels, respectively after 0.5 h or 1 h incubation (n = 4). (g) Release kinetics of MPA from alginate-N_3 gels at pH 5.5 and pH 7.4, respectively (n = 4). Data presented as mean ± SD and analyzed by two-tailed t-test ($0.01 < *P \leq 0.05$; $**P \leq 0.01$; $***P \leq 0.001$).

N_3 gels subsequently released tacrolimus in a pH-dependent manner, with faster release kinetics under pH 5.5 in comparison to pH 7.4 (Fig. 4e). DBCO-hz-tacro loaded alginate-N_3 gels started with a faster rate of release, and reached the steady release phase at an earlier time, in comparison to the DBCO-hz-rapa (Fig. 4c and e).

DBCO-MPA was also successfully covalently captured by alginate-N_3 gels *via* Click chemistry *in vitro*, with a 2.9-fold and 1.5-fold loading increase within 0.5 h and 1 h, respectively in comparison to control alginate gels (Fig. 4f). Alginate-N_3 gels still captured 145% more DBCO-MPA than control gels at 12 h (Fig. S10†). DBCO-MPA conjugated alginate-N_3 gels slowly released MPA over a course of >30 days, and the release of MPA was faster at pH 5.5 compared to pH 7.4 (Fig. 4g). Compared to DBCO-hz-rapa and DBCO-hz-tacro, DBCO-MPA loaded alginate-N_3 gels showed a faster release of drugs in both acidic

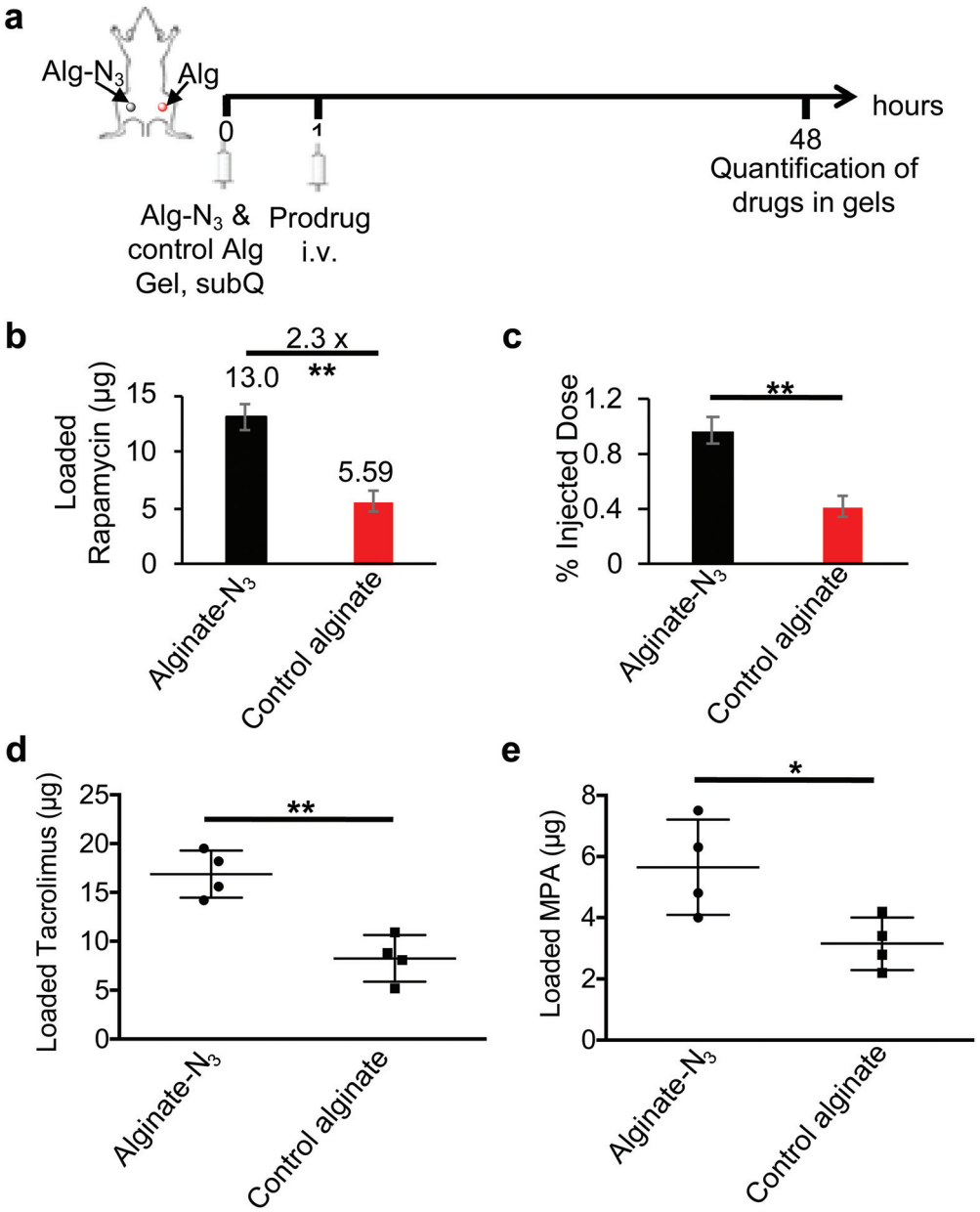

Fig. 5 Targeted loading of DBCO-hz-rapa, DBCO-hz-tacro, and DBCO-MPA to alginate-N_3 gels *in vivo via* click chemistry. (a) Schematic illustration of *in vivo* loading study using mice bearing alginate-N_3 and control alginate gels on different flanks. DBCO-hz-rapa (150 mg kg^{-1}) or DBCO-hz-tacro (150 mg kg^{-1}) or DBCO-MPA (100 mg kg^{-1}) were i.v. injected *via* tail vein, and gels subsequently retrieved to quantify bound prodrugs. (b) Amount of rapamycin recovered from alginate-N_3 or control alginate gels at 48 h post injection (n = 4). (c) Amount of loaded rapamycin in the form of percentage of injected dose (n = 4). (d) Amount of tacrolimus recovered from alginate-N_3 or control alginate gels at 48 h post injection (n = 4). (e) Amount of MPA recovered from alginate-N_3 or control alginate gels at 48 h post injection (n = 4). Data presented as mean ± SD and analyzed by two-tailed t-test ($0.01 < *P \leq 0.05$; $**P \leq 0.01$; $***P \leq 0.001$).

and neutral conditions (Fig. 4c, e, and f), presumably due to the significantly greater hydrophilicity of DBCO-MPA.

The pharmacokinetic properties of DBCO-hz-rapa, DBCO-hz-tacro, and DBCO-MPA were next examined to determine if their circulation times would be sufficiently long to allow for minimally invasive loading onto hydrogel depots, but would be short enough to minimize systemic availability of active drug before clearance of unbound conjugates. Balb/c mice were intravenously (i.v.) injected with prodrugs, and blood was collected for prodrug quantification at different time points. DBCO-hz-rapa was rapidly cleared from the blood, with a blood concentration of 28 μg mL^{-1} (~7% of injected dose (I.D.)) at 1 h post injection (Fig. S11†). The majority of injected DBCO-hz-rapa was cleared from the bloodstream within 9 h (Fig. S11†). For DBCO-hz-tacro, ~11% was retained in the blood after 12 min, and the level dropped to ~1.2% I.D. at 6 h (Fig. S12†). Compared to DBCO-hz-rapa and DBCO-hz-tacro, DBCO-MPA showed a slightly longer retention in the bloodstream, with 7.6% I.D. at 2 h and 3.1% I.D. at 6 h (Fig. S13†), presumably due to the better water-solubility of DBCO-MPA. Compared to DBCO-MPA, free MPA became undetectable within 2 h post intravenous injection, which is consistent with previous reports in rats.[41] For all three prodrugs, the vast majority was cleared from the bloodstream by 12 h (Fig. S11–13†). In clinic, free rapamycin, tacrolimus, and MPA are often orally administered in formulations containing oils or as tablets.[42–44] However, orally administered free drugs suffer from significant gastrointestinal degradation, low total bioavailability, variable pharmacokinetics, and dominant existence of drug–protein complexes in the bloodstream;[42–47] these issues can be potentially addressed by the use of intravenously administered, water-soluble, and anti-fouling prodrugs. Compared to reported drug-encapsulating nanoparticles,[40,48,49] the blood circulation time of DBCO-hz-rapa, DBCO-hz-tacro, and DBCO-MPA is comparable or shorter, which is important to minimize the hydrolysis window of prodrugs and thus the systemic exposure of released free drugs.

We next studied whether alginate-N_3 gels can efficiently capture DBCO-modified immunosuppressive drugs *in vivo*. In the first studies, Balb/c mice were subcutaneously injected with alginate-N_3 or control alginate gels, followed by i.v. injection of DBCO-hz-rapa 1 h later. At 48 h post injection of DBCO-hz-rapa, gels were harvested, disassociated, and treated with acids, prior to quantification of recovered rapamycin *via* LC-MS (Fig. S14a†). Compared to control gels, alginate-N_3 gels retained a significantly higher amount of rapamycin (Fig. S14b and c†), indicating the enhanced capture of DBCO-hz-rapa by alginate-N_3 gels *via* Click chemistry. To further confirm this targeting effect, alginate-N_3 gels and control gels were subcutaneously injected into the left and right flanks of the same Balb/c mice, and after 1 h, DBCO-hz-rapa was i.v. injected *via* tail vein (Fig. 5a). At 48 h post injection of DBCO-hz-rapa, retained rapamycin was quantified and compared. Alginate-N_3 gels were able to capture significantly more DBCO-hz-rapa, as compared to control gels, with a 130% increase in rapamycin retention (Fig. 5b). Approximately 1% of I.D. of DBCO-hz-rapa was retained in alginate-N_3 gels at 48 h post injection, which was significantly higher than control gels (Fig. 5c). Similar studies involving i.v. infusion of DBCO-hz-tacro and DBCO-MPA into Balb/c mice bearing alginate-N_3 and control gels confirmed that both tacrolimus and MPA pro-drugs could be captured by alginate-N_3 gels *in vivo* (Fig. 5d and e). Altogether, these experiments demonstrate that alginate-N_3 gels can covalently capture DBCO-functionalized immunosuppressive drugs *via* efficient Click chemistry *in vivo*. Past studies have demonstrated that click chemistry-mediated targeting efficiency varies with the types of molecules and locations of tissues or biomaterials which are targeted. Molecules that readily diffuse into and are rapidly cleared from target tissues or biomaterials exhibit high targeting efficiency (>100% improvement over non-targeted molecules),[34,39,49] while molecules with a bulky chemical structure and relatively poor pharmacokinetics have shown limited targeting effect (0%–50% improvement).[50–52] The effective targeting of DBCO-hz-rapa (130% improvement), DBCO-hz-tacro (105% improvement) and DBCO-MPA (80% improvement) likely results from their good pharmacokinetics and rapid clearance of uncoupled drug from gels.

Conclusion

We have developed clickable, acid-labile DBCO-hz-tacro, DBCO-hz-rapa and DBCO-MPA for *in vivo* targeted delivery and subsequent controlled, local release of immunosuppressive drugs. These prodrugs enabled covalent conjugation to azido-modified alginate gels, resulting in a sustained, pH-dependent release of active drugs *in vitro*. We further demonstrated that subcutaneously injected alginate-N_3 gels can covalently capture i.v. injected DBCO-hz-tacro, DBCO-hz-rapa and DBCO-MPA. This approach potentially enables targeted delivery of immunosuppressive drugs to biomaterial depots at any time of interest, followed by sustained release of active drugs locally, which is anticipated to flexibly maintain immunosuppression after allotransplantation. Alginate gels as evaluated in our platform are natural non-immunogenic polysaccharides, enable controlled local release of drugs, and are also refillable by binding fresh intravenously injected prodrugs. These gels, once implanted in tissues, do not require replacement every time the drug levels fall to sub-therapeutic thresholds, thus avoiding trauma and inflammation due to repeated gel injections. Further evaluation of the therapeutic benefits of these prodrugs in the context of reconstructive transplantation is underway in animal models.

Methods

Materials and instrumentation

N-β-Maleimidopropionic acid hydrazide (BMPH) was purchased from Thermo Fisher Scientific (Waltham, MA, USA). Rapamycin and tacrolimus were purchased from LC Laboratories (Woburn, MA, USA). MPA was purchased from

Life Technologies Corporation (Chicago, IL, USA). NH_2-PEG_{1k}-SH and NH_2-PEG_{1k}-OH were purchased from Laysan Bio (Arab, AL, USA). DBCO-NHS was purchased from Conju Probe (San Diego, CA, USA). 11-Azido-3,6,9-trioxaundecan-1-amine and other compounds were purchased from Sigma Aldrich (St Louis, MO, USA) unless otherwise noted. PRONOVA UP MVG sodium alginate (endotoxin-free) was purchased from Fmc Biopolymer AS (Sandvika, Norway). Small compounds were run on the Agilent 1290/6140 ultra high performance liquid chromatography/mass spectrometer (LC-MS). Compounds were purified using the Agilent 1200 preparative high performance liquid chromatography (HPLC). Proton nuclear magnetic resonance spectra were collected on the Agilent DD2 600.

Animals

BALB/c mice were purchased from Jackson Laboratory (Bar Harbor, ME, USA). Feed and water were available *ad libitum*. Artificial light was provided in a 12 h/12 h cycle. All procedures involving animals were done in compliance with National Institutes of Health and Institutional guidelines with approval of Harvard University's Institutional Animal Care and Use Committee.

Synthesis of rapamycin-mal

Rapamycin (0.1 mmol) and BMPH (0.12 mmol) were dissolved in methanol, followed by the addition of glacial acetic acid (5 μL). The mixture was stirred at 45 °C for 48 h. After removal of the solvent, the crude product was purified by preparative HPLC to yield rapamycin-mal (60% yield). MS *m*/*z*: calculated for $C_{58}H_{87}N_4O_{15}$ $[M + H]^+$ 1079.6, found 1079.4, calculated for $C_{58}H_{85}N_4O_{15}$ $[M - H]^-$ 1077.6, found 1077.3.

Synthesis of DBCO-PEG_{1k}-SH

NH_2-PEG_{1k}-SH (0.1 mmol) and DBCO-NHS (0.1 mmol) were dissolved in methanol. The mixture was stirred at 37 °C for 24 h. After removal of the solvent, the crude product was stored for use.

Synthesis of DBCO-hz-rapa

Rapamycin-mal (0.1 mmol) and DBCO-PEG_{1k}-SH (0.1 mmol) were dissolved in methanol, followed by the addition of triethylamine (0.1 mmol). The mixture was stirred at 40 °C for 48 h. After removal of the solvent, the crude product was purified *via* preparative HPLC to yield DBCO-hz-rapa.

Synthesis of tacrolimus-mal

Tacrolimus (0.1 mmol) and BMPH (0.12 mmol) were dissolved in methanol, followed by the addition of glacial acetic acid (5 μL). The mixture was stirred at 45 °C for 48 h. After removal of the solvent, the crude product was purified by preparative HPLC to yield tacrolimus-mal (70% yield). MS *m*/*z*: calculated for $C_{52}H_{78}N_3O_{13}$ $[M + H]^+$ 969.5, found 969.4.

Synthesis of DBCO-hz-tacro

Tacrolimus-mal (0.1 mmol) and DBCO-PEG_{1k}-SH (0.1 mmol) were dissolved in methanol, followed by the addition of triethylamine (0.1 mmol). The mixture was stirred at 40 °C for 48 h. After removal of the solvent, the crude product was purified *via* preparative HPLC to yield DBCO-hz-tacro.

Synthesis of MPA-4-nitrophenylcarbonate

MPA (0.1 mmol) and 4-nitrophenyl chloroformate (0.11 mmol) were dissolved in anhydrous dichloromethane, followed by the addition of triethylamine (0.1 mmol). The mixture was stirred at room temperature for 24 h. After removal of the solvent, the crude product was purified *via* preparative HPLC to yield MPA-4-nitrophenylcarbonate (75% yield). MS *m*/*z*: calculated for $C_{24}H_{24}NO_{10}$ $[M + H]^+$ 486.1, found 486.0, calculated for $[2M + Na]^+$ 993.2, found 993.0.

Synthesis of DBCO-PEG_{1k}-OH

NH_2-PEG_{1k}-OH (0.1 mmol) and DBCO-NHS (0.1 mmol) were dissolved in methanol. The mixture was stirred at 37 °C for 24 h. After removal of the solvent, the crude product was purified *via* preparative HPLC.

Synthesis of DBCO-MPA

MPA-4-nitrophenylcarbonate (0.1 mmol) and DBCO-PEG_{1k}-OH (0.1 mmol) were dissolved in dimethylformamide, followed by addition of *N*,*N*-diisopropylethylamine (0.1 mmol) and 4-dimethylaminopyridine (0.1 mmol). The mixture was stirred at room temperature for 48 h. After removal of the solvent, the crude product was purified *via* preparative HPLC to yield DBCO-MPA.

Synthesis of alginate-N_3

Alginate-N_3 was synthesized following the reported procedure.[40] Alginate (1 g) was dissolved in MES buffer, followed by the addition of 11-azido-3,6,9-trioxaundecan-1-amine (160 mg). The mixture was stirred at room temperature for 30 min, and *N*-(3-dimethylaminopropyl)-*N*′-ethylcarbodiimide hydrochloride (EDC·HCl, 160 mg) and hydroxybenzotriazole (HOBt, 140 mg) were then added. The reaction mixture was stirred for another 48 h, adjusted to pH 7.4 using sodium hydroxide solution, placed in a dialysis bag (3.5k MWCO), dialyzed against DI water for 3 days (medium change every 12 h), lyophilized, and stored for use.

Preparation of alginate-N_3 gels

2% (w/v) alginate-N_3 in Dulbecco's Modified Eagle Medium (DMEM, 3 mL) was added into the first syringe, and calcium sulfate slurry (150 μL) was added into the second prepared syringe. Air bubbles were removed, and the syringes were connected by a luer-lock. Solutions were mixed for 20–30 times by pushing plungers back and forth very rapidly. The calcium sulfate slurry was evenly mixed throughout the syringe. For *in vitro* studies, the gels were immediately cast between two silanized glass plates separated by 2 mm spacers. After allowing the gels to cross-link for 45 min, gel disks were punched out using a sterile biopsy punch. For *in vivo* studies, gel solutions (100 μL) were freshly prepared and subcutaneously injected *via* an 18 G needle.

Loading of DBCO-functionalized drugs to alginate-N_3 gels *in vitro*

Alginate-N_3 gels or unmodified alginate gels (2 mm height, 4 mm diameter) in 24-well plates were incubated with DBCO-hz-rapa, DBCO-hz-tacro or DBCO-MPA in DMEM (300 μL, 10 mg mL^{-1}) at 37 °C. At different time points, 10 μL of medium was taken out and diluted with 90 μL of acetonitrile prior to LC-MS analyses. The percentage of prodrug loading was calculated as: (amount of fed prodrugs − amount of remaining prodrugs)/(amount of fed prodrugs). For diffusion study of rapamycin, rapamycin was dissolved in dimethyl sulfoxide prior to addition into the medium.

Release study of drug-loaded gels

Alginate-N_3 gels or control alginate gels previously incubated with DBCO-hz-rapa, DBCO-hz-tacro or DBCO-MPA for 24 h were incubated at 37 °C in fresh DMEM with a pH value of 7.4 and 5.5, respectively. At different time points, 10 μL of medium was taken out and diluted with 90 μL of acetonitrile prior to LC-MS analyses.

Pharmacokinetics study of DBCO-functionalized drugs

DBCO-hz-rapa (50 mg kg^{-1}), DBCO-hz-tacro (50 mg kg^{-1}) or DBCO-MPA (50 mg kg^{-1}) were i.v. administered to Balb/c mice. Blood was collected at different times post injection of DBCO-functionalized drugs, treated with lysis buffer, and centrifuged. Supernatants were collected for quantification of prodrugs *via* LC-MS.

In vivo targeting of DBCO-functionalized drugs

Balb/c mice were subcutaneously injected with alginate-N_3 gels or control gels (100 μL). After 1 h, DBCO-hz-rapa (150 mg kg^{-1}), DBCO-hz-tacro (150 mg kg^{-1}) or DBCO-MPA (100 mg kg^{-1}) were intravenously injected *via* tail vein. At 48 h post injection of DBCO-functionalized drugs, gels were harvested, disrupted using EDTA (10 mM) on ice, and treated with formic acid/acetonitrile to release free drugs. After centrifugation, supernatants were analyzed by LC-MS to quantify the retained drug.

Statistical analyses

Statistical analysis was performed using GraphPad Prism and Microsoft Excel. Sample variance was tested using the F test. For samples with equal variance, the significance between the groups was analyzed by a two-tailed student's t test. For samples with unequal variance, a two-tailed Welch's *t*-test was performed. The results were deemed significant at $0.01 < {}^{*}P \leq 0.05$, highly significant at $0.001 < {}^{**}P \leq 0.01$, and extremely significant at ${}^{***}P \leq 0.001$.

Conflicts of interest

The authors declare no competing financial interests.

Acknowledgements

The studies were supported by funding from the Department of Defense (W81XWH-15-2-0017, Log MR141089) and from National Institutes of Health (1 R01 EB023287, 1 R01 CA223255). H. W. gratefully acknowledges funding support from the Wyss Technology Development Fellowship.

References

1 C. L. Kaufman, *et al.*, Current Status of Vascularized Composite Allotransplantation, *Am. Surg.*, 2019, **85**, 631–637.
2 J. T. Shores, G. Brandacher and W. P. Lee, Hand and upper extremity transplantation: an update of outcomes in the worldwide experience, *Plast. Reconstr. Surg.*, 2015, **135**, 351e–360e.
3 V. S. Gorantla, J. A. Plock and M. R. Davis, *Anesthesia and Perioperative Care for Organ Transplantation*, Springer, New York, 2016, pp. 539–552.
4 C. F. Barker and J. F. Markmann, Historical overview of transplantation, *Cold Spring Harbor Perspect. Med.*, 2013, **3**, a014977.
5 V. S. Gorantla, *et al.*, Immunosuppressive agents in transplantation: mechanisms of action and current anti-rejection strategies, *Microsurgery*, 2000, **20**, 420–429.
6 A. Thomson, C. Bonham and A. Zeevi, Mode of action of tacrolimus (FK506): molecular and cellular mechanisms, *Ther. Drug Monit.*, 1995, **17**, 584–591.
7 T. R. Brazelton, Molecular mechanisms of action of new xenobiotic immunosuppressive drugs: tacrolimus (FK506), sirolimus (rapamycin), mycophenolate mofetil and leflunomide, *Curr. Opin. Immunol.*, 1996, **8**, 710–720.
8 F. J. Dumont and Q. Su, Mechanism of action of the immunosuppressant rapamycin, *Life Sci.*, 1995, **58**, 373–395.
9 S. N. Sehgal, Rapamune®(RAPA, rapamycin, sirolimus): mechanism of action immunosuppressive effect results from blockade of signal transduction and inhibition of cell cycle progression, *Clin. Biochem.*, 1998, **31**, 335–340.
10 M. Poon, *et al.*, Rapamycin inhibits vascular smooth muscle cell migration, *J. Clin. Invest.*, 1996, **98**, 2277–2283.
11 J. E. S. Kitchin, M. K. Pomeranz, G. Pak, K. Washenik and J. L. Shupack, Rediscovering mycophenolic acid: a review of its mechanism, side effects, and potential uses, *J. Am. Acad. Dermatol.*, 1997, **37**, 445–449.
12 A. C. Allison, W. J. Kowalski, C. D. Muller and E. M. Eugui, Mechanisms of action of mycophenolic acid, *Ann. N. Y. Acad. Sci.*, 1993, **696**, 63–87.
13 A. C. Allison and E. M. Eugui, Mechanisms of action of mycophenolate mofetil in preventing acute and chronic allograft rejection, *Transplantation*, 2005, **80**, S181–S190.
14 R. Bentley, Mycophenolic Acid: A One Hundred Year Odyssey from Antibiotic to Immunosuppressant, *Chem. Rev.*, 2000, **100**, 3801–3826.

15 W. Land and F. Vincenti, Toxicity-Sparing Protocols Using Mycophenolate Mofetil in Renal Transplantation, *Transplantation*, 2005, **80**, S221–S234.
16 S. N. Sehgal, Rapamune (Sirolimus, rapamycin): an overview and mechanism of action, *Ther. Drug Monit.*, 1995, **17**, 660–665.
17 S. F. Stewart, M. Hudson, D. Talbot, D. Manas and C. P. Day, Mycophenolate mofetil monotherapy in liver transplantation, *Lancet*, 2001, **357**, 609–610.
18 V. S. Gorantla and A. J. Demetris, Acute and chronic rejection in upper extremity transplantation: what have we learned?, *Hand Clin.*, 2011, **27**, 481–493.
19 E. Brooks, S. E. Tett, N. M. Isbel and C. E. Staatz, Population Pharmacokinetic Modelling and Bayesian Estimation of Tacrolimus Exposure: Is this Clinically Useful for Dosage Prediction Yet?, *Clin. Pharmacokinet.*, 2016, **55**, 1295–1335.
20 R. Bouamar, *et al.*, Tacrolimus predose concentrations do not predict the risk of acute rejection after renal transplantation: a pooled analysis from three randomized-controlled clinical trials(dagger), *Am. J. Transplant.*, 2013, **13**, 1253–1261.
21 G. Brandacher, W. P. Lee and S. Schneeberger, Minimizing immunosuppression in hand transplantation, *Expert Rev. Clin. Immunol.*, 2012, **8**, 673–683.
22 J. T. Schnider, *et al.*, Site-specific immunosuppression in vascularized composite allotransplantation: prospects and potential, *Clin. Dev. Immunol.*, 2013, **2013**, 495212.
23 J. Sellares, *et al.*, Understanding the causes of kidney transplant failure: the dominant role of antibody-mediated rejection and nonadherence, *Am. J. Transplant.*, 2012, **12**, 388–399.
24 G. Janka, S. Imashuku, G. Elinder, M. Schneider and J.-I. Henter, Infection-and malignancy-associated hemophagocytic syndromes: secondary hemophagocytic lymphohistiocytosis, *Hematol. Oncol. Clin.*, 1998, **12**, 435–444.
25 R. T. Bustami, *et al.*, Immunosuppression and the risk of post-transplant malignancy among cadaveric first kidney transplant recipients, *Am. J. Transplant.*, 2004, **4**, 87–93.
26 A. Gutierrez-Dalmau and J. M. Campistol, Immunosuppressive therapy and malignancy in organ transplant recipients, *Drugs*, 2007, **67**, 1167–1198.
27 A. Capron, *et al.*, Correlation of tacrolimus levels in peripheral blood mononuclear cells with histological staging of rejection after liver transplantation: preliminary results of a prospective study, *Transplant Int.*, 2012, **25**, 41–47.
28 F. G. Feturi, *et al.*, Mycophenolic Acid for Topical Immunosuppression in Vascularized Composite Allotransplantation: Optimizing Formulation and Preliminary Evaluation of Bioavailability and Pharmacokinetics, *Front. Surg.*, 2018, **5**, 20.
29 J. T. Schnider, *et al.*, Site-specific immunosuppression in vascularized composite allotransplantation: prospects and potential, *Clin. Dev. Immunol.*, 2013, **2013**, 495212.
30 T. Ruers, W. Buurman, J. Smits, H. Struyker-Boudier and G. Kootstra, Local treatment of renal allografts, a promising way to reduce the dosage of immunosuppressive drugs. Comparison of various ways of administering prednisolone, *Transplantation*, 1986, **41**, 156–161.
31 V. Holan, *et al.*, Cyclosporine A-loaded and stem cell-seeded electrospun nanofibers for cell-based therapy and local immunosuppression, *J. Controlled Release*, 2011, **156**, 406–412.
32 T. Gajanayake, *et al.*, A single localized dose of enzyme-responsive hydrogel improves long-term survival of a vascularized composite allograft, *Sci. Transl. Med.*, 2014, **6**, 249ra110.
33 C. A. Fries, *et al.*, Graft-implanted, enzyme responsive, tacrolimus-eluting hydrogel enables long-term survival of orthotopic porcine limb vascularized composite allografts: A proof of concept study, *PLoS One*, 2019, **14**, e0210914.
34 Y. Brudno, *et al.*, Replenishable drug depot to combat post-resection cancer recurrence, *Biomaterials*, 2018, **178**, 373–382.
35 Y. Brudno, *et al.*, Refilling drug delivery depots through the blood, *Proc. Natl. Acad. Sci. U. S. A.*, 2014, **111**, 12722–12727.
36 E. T. Kool, D.-H. Park and P. Crisalli, Fast hydrazone reactants: electronic and acid/base effects strongly influence rate at biological pH, *J. Am. Chem. Soc.*, 2013, **135**, 17663–17666.
37 S. J. Sonawane, R. S. Kalhapure and T. Govender, Hydrazone linkages in pH responsive drug delivery systems, *Eur. J. Pharm. Sci.*, 2017, **99**, 45–65.
38 J. M. Baskin, *et al.*, Copper-free click chemistry for dynamic in vivo imaging, *Proc. Natl. Acad. Sci. U. S. A.*, 2007, **104**, 16793–16797.
39 H. Wang, *et al.*, Selective in vivo metabolic cell-labeling-mediated cancer targeting, *Nat. Chem. Biol.*, 2017, **13**, 415.
40 Y. Brudno, *et al.*, In Vivo Targeting through Click Chemistry, *ChemMedChem*, 2015, **10**, 617–620.
41 H. Tian, J. Ou, S. C. Strom and R. Venkataramanan, Pharmacokinetics of tacrolimus and mycophenolic acid are altered, but recovered at different times during hepatic regeneration in rats, *Drug Metab. Dispos.*, 2005, **33**, 329–335.
42 K. Mahalati and B. D. Kahan, Clinical Pharmacokinetics of Sirolimus, *Clin. Pharmacokinet.*, 2001, **40**, 573–585.
43 D. Zhang and D. S.-L. Chow, Clinical Pharmacokinetics of Mycophenolic Acid in Hematopoietic Stem Cell Transplantation Recipients, *Eur. J. Drug Metab. Pharmacokinet.*, 2017, **42**, 183–189.
44 R. Venkataramanan, *et al.*, Clinical Pharmacokinetics of Tacrolimus, *Clin. Pharmacokinet.*, 1995, **29**, 404–430.
45 A. MacDonald, J. Scarola, J. T. Burke and J. J. Zimmerman, Clinical pharmacokinetics and therapeutic drug monitoring of sirolimus, *Clin. Ther.*, 2000, **22**, B101–B121.
46 M. Antignac, B. Barrou, R. Farinotti, P. Lechat and S. Urien, Population pharmacokinetics and bioavailability of tacrolimus in kidney transplant patients, *Br. J. Clin. Pharmacol.*, 2007, **64**, 750–757.

47 T. Shirasu, *et al.*, Nanoparticles Effectively Target Rapamycin Delivery to Sites of Experimental Aortic Aneurysm in Rats, *PLoS One*, 2016, **11**, e0157813–e0157813.
48 S.-B. Shin, H.-Y. Cho, D.-D. Kim, H.-G. Choi and Y.-B. Lee, Preparation and evaluation of tacrolimus-loaded nanoparticles for lymphatic delivery, *Eur. J. Pharm. Biopharm.*, 2010, **74**, 164–171.
49 T. Solymosi, *et al.*, Sirolimus formulation with improved pharmacokinetic properties produced by a continuous flow method, *Eur. J. Pharm. Biopharm.*, 2015, **94**, 135–140.
50 H. Wang, *et al.*, In vivo cancer targeting via glycopolyester nanoparticle mediated metabolic cell labeling followed by click reaction, *Biomaterials*, 2019, 119305.
51 H. Wang, *et al.*, Targeted Ultrasound-Assisted Cancer-Selective Chemical Labeling and Subsequent Cancer Imaging using Click Chemistry, *Angew. Chem., Int. Ed.*, 2016, **55**, 5452–5456.
52 H. Wang, *et al.*, In Vivo Targeting of Metabolically Labeled Cancers with Ultra-Small Silica Nanoconjugates, *Theranostics*, 2016, **6**, 1467–1476.